13

Biarticular Actuation of Robotic Systems

Jan Babič
"Jožef Stefan" Institute
Slovenia

1. Introduction

In biology, biarticular muscles are muscles that are passing two joints. One of the biarticular muscles that is passing the knee and the ankle joints is the Gastrocnemius muscle (see Fig. 1). Functions of the biarticular muscles during human movement have been studied extensively by many researchers but these functions still remain unclear. One of such functions is the transportation of mechanical energy from proximal to distal points (Ingen Schenau, 1989). It is believed that this transportation causes an effective transformation of rotational motion of body segments into translation of the body centre of gravity. The mechanism by which this is achieved is the timely activation of biarticular muscles before the end of the explosive phase of the movement. The activation of the biarticular muscle prior to the end of the explosive phase of the motion enables the transportation of the power generated by the proximal joint extensors from the proximal joint to the distal joint. This transfer of mechanical energy can be explained using the following example of the gastrocnemius muscle activation. During the push-off phase of the human jump, the knee joint is rapidly extended as a result of the positive work done by the knee extensor muscles. If the biarticular gastrocnemius muscle contracts isometrically (its length does not change), the additional mechanical work is done at the ankle joint because of the gastrocnemius muscle, which contributes no mechanical work by itself. A part of the energy generated by the knee extensors appears as mechanical work at the ankle joint and the height of the jump is significantly increased. This is because, as the jump proceeds and the knee straightens, the angular position changes of the knee have progressively less effect on vertical velocity of the jumper centre of gravity. By gastrocnemius muscle activation, a rapid extension of the foot is produced. This extension has a greater effect on the vertical velocity than the extension of the almost straightened knee. The energy is more effectively translated into vertical velocity and a greater height of the jump is achieved. However, the timing of the gastrocnemius muscle activation is critical to obtain a maximum effect. This was demonstrated by an articulated physical model of the vertical jump by Bobbert et al (1986).
Besides biarticularity, the gastrocnemius muscle has one more interesting feature. It is connected to the foot by an elastic tendon (see Fig. 1). The elasticity in the muscle fibres and tendons plays an important role in enhancing the effectiveness and the efficiency of human performance. An enhanced performance of human motion has been most effectively demonstrated for jumping and running (Cavagna, 1970; Bobbert et al., 1996; Shorten, 1985; Hobara, 2008). An important feature of elastic tissues is the ability to store elastic energy when stretched and to recoil this energy afterwards as a mechanical work (Asmussen and

Bonde-Petersen, 1974). Beside this feature, oscillatory movements performed at the natural frequency of muscle-tendon complex could maximize the performance. A countermovement vertical jump can be treated as one period of oscillatory movement and from this point of view the natural frequency, as well as parameters that define the natural frequency, can be determined.

Lower extremities of today's humanoid robots are mostly serial mechanisms with simple rotational joints that are driven directly or indirectly by electrical servo drives. Such design of humanoid robot mechanism allows only rotational motion in joints to occur. This means that translations of the robot's centre of gravity are solely a result of the transformation of rotations in joints into translations of the robot centre of gravity. Especially in ballistic movements such as fast running or jumping where the robot centre of gravity is to be accelerated from low or zero velocity to a velocity as high as possible, this transformation is handicapped. The transfer of the angular motion of the lower extremity segments to the desired translational motion of the robot centre of gravity is less effective the more the joints are extended. When the joint is fully extended, the effect of this joint on the translational motion of the robot centre of gravity in a certain direction equals zero. Besides, the motion of the segments should decelerate to zero prior to the full extension to prevent a possible damaging hyperextension. Where relatively large segments which may contain considerable amounts of rotational energy are involved, high power is necessary to decelerate the angular motion.

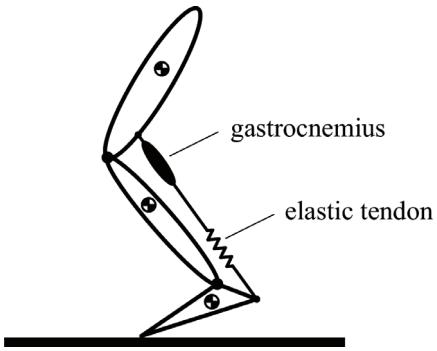

Fig. 1. Biarticular muscle gastrocnemius passing the knee and the ankle joints. It acts as a knee flexor and ankle extensor. Gastrocnemius muscle is connected to the foot by an elastic tendon

The purpose of this chapter is, first, to make an extensive review of the research of the role of biarticular muscles in motion of the humans and to present this biomechanical body of knowledge from an engineering perspective, and second, to describe the research results where biarticular actuation was used to achieve energy efficient and high performance motion of a humanoid robotic leg. The chapter is based mostly on the previous journal publications of the author and on the yet unpublished research results.

2. Role of biarticular muscles in human jump

Vertical jumping is a complex task requiring quick and harmonized coordination of jumper's body segments, first for the push-off, then for the flight and lastly for the landing.

The prime criterion for vertical jump efficiency is the height of the jump that depends on the speed of the jumper's centre of gravity (COG) in the moment when the feet detach from the ground. Besides maintaining the balance, the task of the muscles during the push-off phase of the jump is to accelerate the body's COG up in the vertical direction to the extended body position. During the push-off phase of the jump, the jumper's centre of gravity must be above the supporting polygon that is formed by the feet (Babič et al., 2001). In contrast to the humans, today's humanoid robots are mostly unable to perform fast movements such as the vertical jump. They can mostly perform only slow and statically stable movements that do not imitate the human motion. Besides, these slow and statically stable movements are energy inefficient. With the understanding of the anatomy and the biomechanics of the human body, one can find out that, beside the shape, majority of today's humanoid robots and human bodies do not have a lot of common properties. To achieve a better imitation of the human motion and ability to perform fast movements such as the vertical jump or running, other properties and particularities, beside the shape of the body, should be considered in the design of the humanoid robot.
In this section we will first analyse the human vertical jump and show that for each and every subject there exists an optimal triceps surae muscle-tendon complex stiffness that ensures the maximal possible height of the vertical jump. We define the influence of the m. gastrocnemius activation timing and the m. gastrocnemius and Achilles tendon stiffness on the height of the vertical jump and establish the methodology for analysis and evaluation of the vertical jump. We monitored kinematics, dynamics and m. gastrocnemius electrical activity during the maximum height countermovement jump of human subjects and measured viscoelastic properties of the m. gastrocnemius and Achilles tendon using the free-vibration technique. Based on the findings of the biomechanical study of the human vertical jump we performed a simulation study of the humanoid robot vertical jump. As a result we propose a new human inspired structure of the lower extremity mechanism by which a humanoid robot would be able to efficiently perform fast movements such as running and jumping.

2.1 Biorobotic model of vertical jump

Biorobotic model of the vertical jump consists of the dynamic model of the musculoskeletal system and of the mathematical model used for the motion control of the model. The results of the modelling are differential equations and a diagram for simulation and optimization of the vertical jump.

2.1.1 Dynamic model of musculoskeletal system

Vertical jump is an example of a movement that can be satisfactorily observed and analysed in just a sagittal plane. Therefore we built a model of the musculoskeletal system in a two dimensional space of the sagittal plane. Because both lower extremities perform the same movement during the vertical jump, we joined both extremities in one extremity with three rigid body segments. Trunk, head and upper extremities were modelled as one rigid body with a common COG, mass and moment of inertia. The model of the musculoskeletal system is therefore a planar model composed of four segments that represent the foot, shank, thigh and trunk together with the head and both upper extremities. Segments of the model are joined together by frictionless rotational hinges whose axes are perpendicular to the sagittal plane. The contact between the foot and the ground is modelled as a rotational

joint between the tip of the foot and the ground. A model, whose foot is connected to the ground by a rotational joint, is applicable only for the push-off and landing phases of the vertical jump and is not applicable for the flight. As the motion of the COG during the flight is simply described and depends only on the speed vector of the COG just prior to the take-off, this simplification does not present any limitations.

Fig. 2 shows the planar model of the musculoskeletal system, composed of four rigid bodies that represent the foot, shank, thigh and trunk together with the head and both upper extremities. The origin of the base coordinate system is in the centre of the virtual joint that connects the foot with the ground.

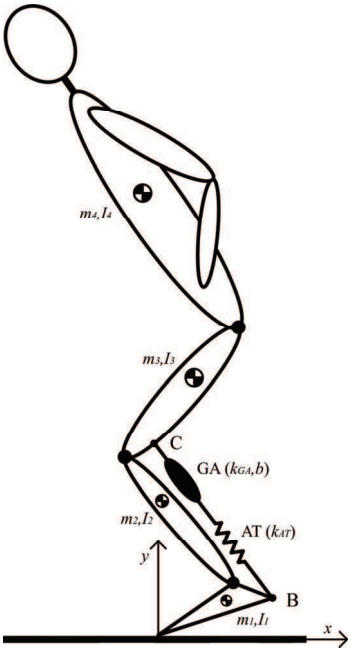

Fig. 2. Planar model of the musculoskeletal system

Passive constraints in the hip, knee and ankle that define the range of motion of these joints were modelled as simple nonlinear springs (Audu and Davy, 1985; Davy and Audu, 1987).

Fig. 2 also shows the model of the biarticular link that consists of the gastrocnemius muscle (GA) with stiffness k_{GA} and damping b and the Achilles tendon (AT) with stiffness k_{AT}. Contrary to the real gastrocnemius muscle, biarticular link cannot contract. It can only be enabled or disabled at different moments during the push-off phase of the jump. High pennation angle of the gastrocnemius muscle fibres suggest that the predominant role of the m. gastrocnemius is not in its contraction but in its ability to bear high forces and to enable the energy transportation from the knee to the ankle (Bogert et al., 1989; Legreneur et al., 1997). Therefore our simulated biarticular link that cannot contract and can only be enabled or disabled is considered as an appropriate model for this study.

Insertions of the biarticular link on the foot (B) and thigh (C) have been determined from the muscle data provided by Brand et al. (1982) and Delp (1990).

Vector of the force in the biarticular link $\boldsymbol{f}$ is

$$\boldsymbol{f} = k \cdot (\boldsymbol{BC} - \boldsymbol{BC}_0) - b \cdot \dot{\boldsymbol{BC}}\,, \tag{1}$$

where k represents the stiffness of the m. gastrocnemius and Achilles tendon connected in series, $\boldsymbol{BC}$ is the vector between the insertions of the biarticular link on the foot and thigh. $\boldsymbol{BC}_0$ is the vector $\boldsymbol{BC}$ in the moment of the gastrocnemius muscle activation. Force in the biarticular link $\boldsymbol{f}$ causes a torque in the ankle joint

$$Q_{bl\,2} = -\left\| \boldsymbol{r}_B \times \boldsymbol{f} \right\|, \tag{2}$$

where $\boldsymbol{r}_B$ is the moment arm vector from the centre of the ankle joint to the insertion of the biarticular link on the foot and a torque in the knee joint

$$Q_{bl\,3} = \left\| \boldsymbol{r}_C \times \boldsymbol{f} \right\|, \tag{3}$$

where $\boldsymbol{r}_C$ is the moment arm vector from the centre of the knee joint to the insertion of the biarticular link on the thigh.
Motion of the musculoskeletal system is written with a system of dynamic equations of motion

$$\mathbf{H}(\boldsymbol{q})\ddot{\boldsymbol{q}} + \boldsymbol{h}(\boldsymbol{q}, \dot{\boldsymbol{q}}) + \boldsymbol{G}(\boldsymbol{q}) = \boldsymbol{Q}_{mov} + \boldsymbol{Q}_{pas} + \boldsymbol{Q}_{bl}\,, \tag{4}$$

where $\boldsymbol{Q}_{pas}$ is the vector of joint torques caused by the passive constraints in the joints and $\boldsymbol{Q}_{bl}$ is the vector of joint torques caused by the biarticular link. $\boldsymbol{Q}_{mov}$ is the vector of joint torques caused by muscles and represents the input to the direct dynamic model of the musculoskeletal system. The output from the direct dynamic model is the vector of joint displacements $\boldsymbol{q}$. We determined parameters of (4) $\mathbf{H}(\boldsymbol{q}), \boldsymbol{h}(\boldsymbol{q}, \dot{\boldsymbol{q}}), \boldsymbol{G}(\boldsymbol{q})$ using the equations published by Asada and Slotine (1986). Simulation diagram of the direct dynamic model of the musculoskeletal system is shown in the shaded rectangle of the Fig. 3.

2.1.2 Motion control

Motion controller of the musculoskeletal system was designed to meet the following four requirements:

1. Perpendicular projection of the body's COG on the ground coincides with the virtual joint that connects the foot with the ground during the entire push-off phase of the vertical jump. Therefore balance of the jumper and verticality of the jump is assured. Equation that describes this requirement is

$$x_T^d(t) = 0\,, \tag{5}$$

   where $x_T^d(t)$ is the distance between the desired perpendicular projection of the body's COG on the ground from the origin of the base coordinate system in time t.
2. Motion controller assures the desired vertical movement of the body's COG relative to the ankle $y_{TA}^d(t)$. By controlling the movement of the body's COG relative to the ankle, we excluded the influence of the biarticular link on the motion $y_{TA}^d(t)$. Therefore parameters of the biarticular link can be varied and optimized for a certain desired motion of the body's COG relative to the ankle.

3. Motion controller assures a constant angle of the foot relative to the ground q_1 before the biarticular link activation occurs. Thus the number of degrees of freedom of the model remains constant during the push-off phase of the vertical jump
4. In the moment, when the biarticular link activates, motion controller sets the torque in the ankle joint Q_2 to zero and thus enable a free motion of the foot relative to the ground. By setting the torque in the ankle joint to zero, the motion in the ankle joint is only a function of the motion in the knee joint that is transmitted to the ankle by the biarticular link.

Motion controller that considers the requirement (5) and enables the desired vertical motion of the COG relative to the ankle $y_{TA}^{d}(t)$ in the base coordinate system is

$$\ddot{\boldsymbol{x}}_T^c = \begin{bmatrix} 0 \\ \ddot{y}_{TA}^d + \ddot{y}_A \end{bmatrix} + k_p \left(\begin{bmatrix} 0 \\ y_{TA}^d + y_A \end{bmatrix} - \boldsymbol{x}_T \right) + k_d \left(\begin{bmatrix} 0 \\ \dot{y}_{TA}^d + \dot{y}_A \end{bmatrix} - \dot{\boldsymbol{x}}_T \right), \tag{6}$$

where k_p and k_d are coefficients of the PD controller, $\ddot{\boldsymbol{x}}_T^c$ is the vector of the control acceleration of the COG in the base coordinate system, y_A is the current height of the ankle joint relative to the ground, $\dot{\boldsymbol{x}}_T, \boldsymbol{x}_T$ are the vectors of the current speed and position of the COG in the base coordinate system.

The relation between the vector of the control speed of the COG in the base coordinate system $\dot{\boldsymbol{x}}_T^c$ and the vector of the control angular velocities in the joints $\dot{\boldsymbol{q}}_c$ is

$$\dot{\boldsymbol{x}}_T^c = \mathbf{J}_T \dot{\boldsymbol{q}}_c, \tag{7}$$

where $\mathbf{J}_T$ is the Jacobian matrix of the COG speed in the base coordinate system. Equation (7) represents an under determined system of equations. From the requirement that the motion controller assures a constant angle of the foot relative to the ground q_1 before the biarticular link activation occurs, follows the condition

$$\dot{q}_{c1} = 0. \tag{8}$$

An additional condition that abolishes the under determination of (7) is the relationship of the knee and hip joint angles

$$\dot{q}_{c4} = n \cdot \dot{q}_{c3}, \tag{9}$$

where n is the coefficient that describes the relationship.

By substitution of (8) and (9) into (7) we get a relation between the vector of the control speed of the COG in the base coordinate system $\dot{\boldsymbol{x}}_T^c$ and the vector of the control angular velocities in the ankle and knee joints $\dot{\boldsymbol{q}}_c'$

$$\dot{\boldsymbol{x}}_T^c = \mathbf{J}_\mathbf{T}' \dot{\boldsymbol{q}}_c', \tag{10}$$

where $\mathbf{J}_\mathbf{T}'$ is a new Jacobian matrix of the centre of gravity speed in the base coordinate system. Differentiation of (10) with respect to time yields

$$\ddot{\boldsymbol{q}}_c' = \begin{bmatrix} \ddot{q}_{c2} \\ \ddot{q}_{c3} \end{bmatrix} = \mathbf{J}_T'^{-1} (\ddot{\boldsymbol{x}}_T^c - \dot{\mathbf{J}}_T' \dot{\boldsymbol{q}}'), \tag{11}$$

where

$$\dot{\boldsymbol{q}}' = \begin{bmatrix} \dot{q}_2 \\ \dot{q}_3 \end{bmatrix}. \tag{12}$$

On the basis of conditions (8) and (9) and relation (11) we define control angular accelerations in all four joints

$$\ddot{\boldsymbol{q}}_c = \begin{bmatrix} 0 \\ \ddot{q}_{c2} \\ \ddot{q}_{c3} \\ n\ddot{q}_{c3} \end{bmatrix}. \tag{13}$$

By substitution of (13) into a system of dynamic equations of motion (4) we get control torques in joints $\boldsymbol{Q}_{mov}$ that we need to control the model of the musculoskeletal system

$$\boldsymbol{Q}_{mov} = \mathbf{H}(\boldsymbol{q})\ddot{\boldsymbol{q}}_c + \boldsymbol{h}(\boldsymbol{q}, \dot{\boldsymbol{q}}) + \boldsymbol{G}(\boldsymbol{q}). \tag{14}$$

Direct dynamic model of the musculoskeletal system together with the motion controller compose the biorobotic model of the vertical jump. Simulation diagram for the simulation of the vertical jump is shown in Fig. 3. Inputs into the simulation diagram are the desired trajectory of COG relative to the ankle y_{TA}^d and a signal for biarticular link activation a. Output from the simulation diagram is the vector of body's COG position $\boldsymbol{x}_T$.

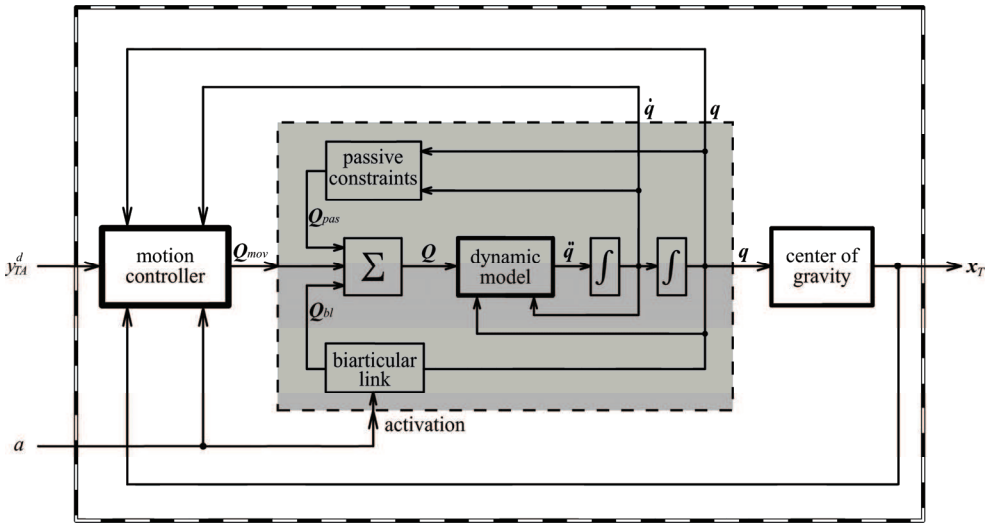

Fig. 3. Simulation diagram for the simulation of the vertical jump. Inputs into the simulation diagram are the desired trajectory of the COG relative to the ankle and a signal for biarticular link activation. Output from the simulation diagram is the vector of jumper's COG position

2.2 Biomechanical analysis of human vertical jump

2.2.1 Subjects and experimental protocol

Ten trained male subjects (age 26 ± 4 years, height 180.3 ± 6.56 cm, body mass 77.1 ± 7.24 kg) participated in the study. Informed consent was obtained from all of them. The protocol of the study was approved by the National Ethics Committee of the Republic of Slovenia. The experiments comply with the current laws of the Republic of Slovenia.

After a warm-up procedure and three practice jumps, subjects subsequently performed four countermovement vertical jumps. They were instructed to keep their hands on the hips and to jump as high as possible. At the beginning of each vertical jump, subjects stood on their toes and in the erected position. During each jump, position of anatomical landmarks over epicondylus lateralis and fifth metatarsophalangeal joint were monitored, ground reaction forces were measured and electromyogram of m. gastrocnemius was recorded. After the jumping, we determined viscoelastic properties of the triceps surae muscle tendon complex of all subjects. Details on methods and procedures are provided in the following sections.

2.2.2 Anthropometric measurements

Segmental anthropometric parameters, such as masses, moments of inertia about the transverse axes, lengths and locations of the centres of gravity were estimated using regression equations (Zatsiorsky and Seluyanov 1983; Leva 1996). Position of the first metatarsophalangeal joint and the Achilles tendon insertion on the calcaneus were determined by palpation for each subject. Insertion of the m. gastrocnemius on femur was determined using the muscle data collected by Brand et al. (1982) and Delp (1990).

2.2.3 Kinematics and dynamics

To determine the motion of the body's COG during the vertical jump we measured the vertical component of the ground reaction force caused by the subject during the jump. Subjects performed vertical jumps on a force platform (Kistler 9281CA) that is capable to measure ground reaction forces with the frequency of 1000 Hz. We zeroed the force platform just prior to the vertical jump when the subject was standing still in the erected position. Thus we enabled the precise determination of the subject's body mass. Body mass of the subject standing on the force platform is therefore equal to the quotient between the negative ground reaction force during the flight phase of the jump and the ground acceleration. The vertical position of the body's COG relative to the ground in time t $y_T^m(t)$ was obtained by double integrating with respect to time the vertical ground reaction force in time t $F(t)$

$$y_T^m(t) = \frac{1}{m}\int_0^t\int_0^t F(t)dtdt + y_T^m(0) \tag{15}$$

where m is the body mass of the subject and $y_T^m(0)$ is the initial height of the body's COG relative to the ground. To determine the vertical position of the body's COG relative to the ankle in time t $y_{TA}^m(t)$ we measured the motion of the ankle during the vertical jump by means of the contactless motion capture system (eMotion Smart). The vertical position of the body's COG relative to the ankle is therefore

$$y_{TA}^{m}(t) = y_{T}^{m}(t) - y_{A}^{m}(t) \tag{16}$$

where $y_{A}^{m}(t)$ is the vertical position of the ankle in time t.

2.2.4 Electromyography

The activity of the m. gastrocnemius was recorded using a pair of surface electrodes put over the medial head of the m. gastrocnemius. Analogue EMG signals were amplified and filtered with a band-pass filter with cut off frequencies at 1 Hz and 200 Hz. The signals were then digitalized with 1000 Hz sampling frequency and full-wave rectified. To reduce the variability of sampled EMG signal, the signal was then smoothed with a digital low-pass Butterworth filter. Finally the EMG signal was normalized with respect to the maximum value attained during the vertical jump.

2.2.5 Measurements of muscle-tendon viscoelastic properties

Triceps surae muscle-tendon complex viscoelastic properties of both legs were measured for each subject using the free-vibration method described by Babič and Lenarcič (2004). The measurement device and the procedure have been designed in such a manner that as few human body segments move as possible during the measurement. Thus the measurement uncertainty due to the approximation of the properties of the human body segments was minimized. The results of the measurements are the elastic stiffness k_{GA} and viscosity b of the m. gastrocnemius and the elastic stiffness k_{AT} of the Achilles tendon.

2.2.6 Treatment of data

For the purposes of analysis and optimization of the vertical jump we adjusted the biomechanical model of the musculoskeletal system with segmental anthropometric parameters, such as masses, moments of inertia about the transverse axes, lengths and locations of the centers of gravity of each subject. Parameters of the biarticular link, such as insertion of the m. gastrocnemius on femur, insertion of the Achilles tendon on calcaneus, elastic stiffness and viscosity were adjusted to match the measured parameters of each subject.

To simulate the vertical jump of the individual subject we used the measured trajectory of the body's COG as the input into the biomechanical model of the vertical jump. Biarticular link activation that is also an input into the biomechanical model of the vertical jump was determined from the EMG signal of the m. gastrocnemius. The moment of biarticular link activation was determined as the moment when the rectified, normalized and filtered EMG signal of the m. gastrocnemius increased to 95% of its maximum value. After the activation, the biarticular link remains active during the entire push-off phase of the jump.

2.2.7 Results

To determine the optimal timing of the biarticular link activation that results in the highest vertical jump, a series of the countermovement vertical jump simulations have been performed for each subject. Each simulation was performed with a different timing of the biarticular link activation.

All subjects activated their m. gastrocnemius slightly before the optimal moment, determined by means of simulations. In average, the difference between the optimal and measured knee angle when the m. gastrocnemius was activated was 6.4 ± 2.22°. Because the

dynamic model of the musculoskeletal system does not include the monoarticular muscle soleus, the measured heights of the jumps were higher than the jump heights determined with the simulations for 4.3 ±1.12 % in average. The primary motive for omitting the m. soleus from the modelling is that we wanted to control the motion of the body's COG relative to the ankle so that the parameters of the biarticular link could be varied and optimized for a certain measured motion of the subject's COG relative to the ankle. If the dynamic model of the musculoskeletal system would include the m. soleus, the motion of the ankle would be fully determined by the force of the m. soleus and we would not be able to control it with regard to the desired body's COG relative to the ankle. Moreover if the dynamic model of the musculoskeletal system would include the m. soleus, force produced by the m. soleus would be another input into the biomechanical model of the vertical jump and we would have to accurately measure the force produced by the m. soleus of subjects performing the vertical jump. An additional cause for the differences between the measured heights of the jumps and the jump heights determined by means of simulations can be the simplified model of the foot that we modelled as one rigid body. The arch of the foot is linked up by elastic ligaments that can store elastic energy when deformed and later reutilize it as the mechanical work (Alexander, 1988). Ker et al. (1987) measured the deformation of the foot during running and determined the amount of the energy stored during the deformation. They showed that the elasticity of the foot significantly contribute to the efficiency of the human movement. To be able to compare the measurements and the simulation results, we corrected the simulation results by adding the contribution of the m. soleus to the height of the vertical jump. Such corrected heights of the vertical jumps at the optimal moments of m. gastrocnemius activation are insignificantly larger than the measured heights of the vertical jumps for all subjects. In average the height difference is only 1.6 ± 0.74 cm.

To determine the optimal stiffness of the Achilles tendon regarding to the height of the vertical jump, a series of the countermovement vertical jump simulations have been performed, each with a different stiffness of the Achilles tendon. Optimal timing of the biarticular link has been determined for each stiffness of the Achilles tendon as described in the previous paragraph. The measured values of the Achilles tendon stiffness for all subjects were always higher than the optimal values determined by means of simulations. By considering the elastic properties of the arch of the foot, we can assume that the optimal values of the Achilles tendon stiffness would increase and therefore the differences between the optimal and measured values would decrease.

Results of the measurements, simulations and optimizations of the human vertical jumps are presented in Fig. 4. Subjects are arranged with regard to the ratio between the optimal stiffness of the Achilles tendon determined by means of simulations and the measured stiffness of the Achilles tendon. If we want to evaluate the contribution of the viscoelastic properties to the height of the jump, ranking of the subjects with regard to the height of the jump is not appropriate because the main parameter that influences the height of the vertical jump is the power generated by muscles during the push-off phase of the jump. The elasticity of the Achilles tendon has the secondary influence on the height of the jump. Results show that for the same power generated by an individual subject during the push-off phase of the jump, the height of the vertical jump varies with the Achilles tendon stiffness. Therefore the appropriate criterion for ranking the subjects have to consider the elasticity of the Achilles tendon.

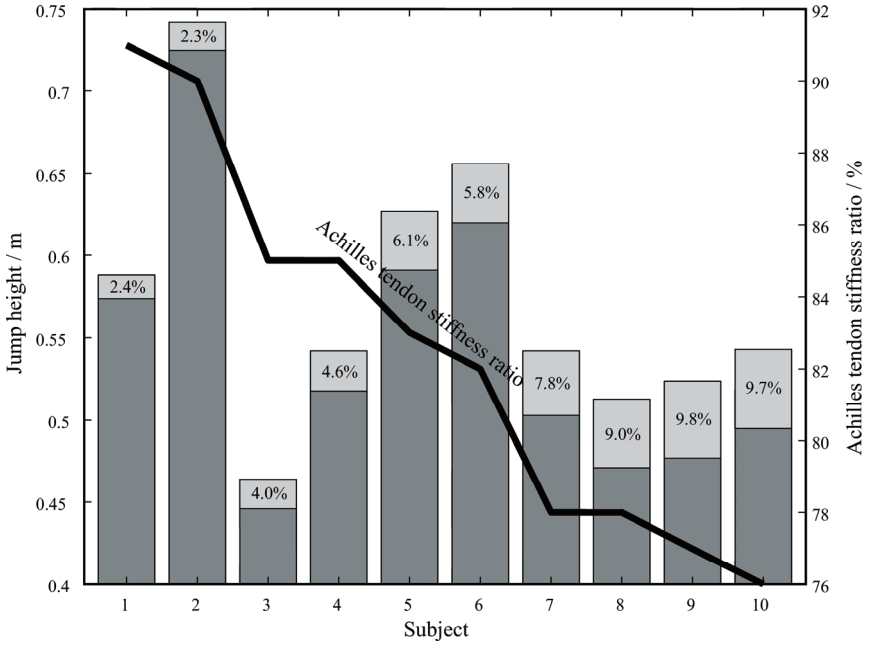

Fig. 4. Results of the measurements, simulations and optimizations of the vertical jumps. Whole bars represent the maximal heights of the vertical jumps achieved with the optimal values of the Achilles tendon stiffness and determined by means of simulations. The dark shaded parts of the bars represent the measured heights of the vertical jumps while the light shaded tops represent the differences between the maximal and measured heights of the vertical jumps. The differences are also shown as percentages relative to the measured heights. Bold line represents the ratio between the optimal stiffness of the Achilles tendon determined by means of simulations and the measured stiffness of the Achilles tendon for each subject

3. Biarticular legged robot

In the past, several research groups developed and studied jumping robots but most of these were simple mechanisms not similar to humans. Probably the best-known hopping robots were designed by Raibert and his team (Raibert, 1986). They developed different hopping robots, all with telescopic legs and with a steady-state control algorithm. Later, De Man et al. developed a trajectory generation strategy based on the angular momentum theorem which was implemented on a model with articulated legs (De Man et al., 1996). Hyon et al. developed a one-legged hopping robot with a structure based on the hind-limb model of a dog (Hyon et al., 2003). Recently, Iida et al. investigated a model of biped robot which makes use of minimum control and elastic passive joints inspired by the structures of biological systems (Iida et al., 2009).

We built an efficient dynamic model of the humanoid robot and designed and built a human inspired half sized humanoid robotic mechanism that is capable of performing vertical jump and long jump. We describe the complete design process of the real robotic

system. Besides, we describe the controller of the robot and show the results of the vertical jump experiments performed by the hardware prototype of the robot.

3.1 Design and specifications

To perform explosive movements such as the vertical jump, very high torques in the robot's joints are required in addition with the low mass of the whole system. To achieve high joint torque with a lightweight electromotor available on the market today, high gear ratio is usually necessary. However, high gear ratio is not desired because we want to maintain the friction in the joints as low as possible. Besides, the back drivability of the joints, where the joints can be easily moved by an external force, cannot be achieved using gears with high ratio. A suitable method to achieve high torques and back drivability at the same time is to use a motor with low gear ratio and overload it for the short periods of time when the high torque is needed. This allows us to get a sufficient torque for a shorter time, that depends on the cooling situation and the desired overloaded torque. Explosive movements such as vertical jump usually last a very brief period of time. Therefore this overloading method seems appropriate for our task.

We used Maxon RE 40 DC servo drives with stall torque of 2.5 Nm and weight of only 480 g. The gear ratio we chose is 1:8, which ensures both low friction and back drivability of the joint. Using this motor/gear combination, the maximal joint torque is 20 Nm, which can, based on the simulations, be sufficient to perform a 20cm high vertical jump.

Each joint is activated by a servo drive mounted inside the proximal segment with regard to the joint. The largest part of the robot weight is in the trunk segment where, besides the motor that activates the hip joint, a computer, a motion controller, all power amplifiers and an inclinometer are installed. To have a heavy trunk is not desired from a control point of view. However, it can be shown that this kind of weight distribution can be beneficial for improvement of fast and explosive movements such as the vertical jump.

The biarticular actuation mechanism is attached between the thigh and heel as in the simulation model. It is realized by a stiff steel wire of diameter 1mm that is connected to the heel via a spring. The spring is interchangeable – springs of varying stiffness determined by measurements are available. At one end the steel wire is wound on a 10mm diameter grooved shaft that is directly connected to a flat servo motor (the spiral groove prevents the wire from knotting itself). This motor functions solely as a break: when the motor is not activated the biarticular link smoothly follows the motion of the robot (the force in the biarticular link is zero).

3.1.1 Construction

The real robotic system was constructed considering the CAD model built in I-DEAS. The real robotic system and its comparison with the CAD model is shown in Fig. 5. All mechanical parts are made of aluminium except the gears and axes that are made of titanium. The total weight of the robot is approximately 4.4 kg and its height is 972mm.

To better understand the biarticular actuation mechanism, consider a jumping motion starting from a squat position. Until the instant of activation, the biarticular actuation mechanism has no effect on the system, essentially acting as a passive prismatic joint. When the biarticular actuation mechanism is activated, the robot essentially becomes redundantly actuated by the biarticular force. Immediately after robot pushes off the ground, the

biarticular actuator is deactivated. This sequence must be executed over a short time in an optimal fashion to maximize jump performance.

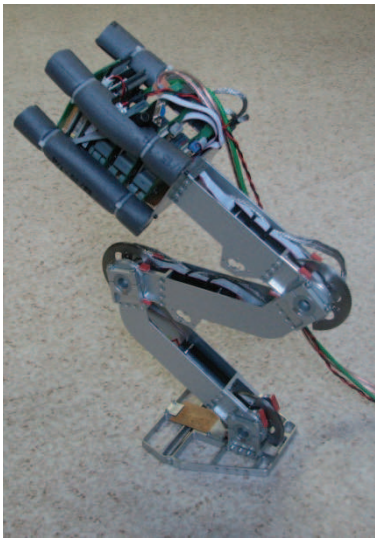

Fig. 5. Real jumping robot

3.2 Dynamic modelling

To efficiently control the robot we determined the dynamic model of the robot. We approximated the robotic system as a planar articulated system composed of four rigid bodies connected together by three rotational joints. To define the dynamic model of the robot, all kinematic and dynamic properties of the robot segments have to be determined. We determined these parameters using I-DEAS modeling software. To increase the accuracy of the model, the weights that we obtained from the I-DEAS model were further adjusted by the measured weights of the manufactured parts.
The obtained properties of all four links including servo drives, computer, power amplifiers and wirings are shown in Table 1.

link	mass kg	length mm	COM position mm	Inertia kgmm^2
foot	0.399	93.5	70.7, -3.4	1057
shank	0.963	255	127.8, 10.5	7487
thigh	1.033	254	119.2, -12.0	7440
trunk	2.031	370	186.4, -12.0	20366

Table 1. Kinematic and dynamic properties of the robot links

The dynamic model of the robot was used in the simulation of the robotic system and for the control of the real system.
The dynamic model is a combination of two separate models, the model of the robot in contact with the ground and the model of the robot in the air. The contact between the tip of

the foot and the ground is modeled as a rotational hinge joint between the foot tip and the ground. With the assumption that the foot tip does not slip and does not bounce, the robot has four degrees of freedom during stance. While in the air, the robot has two more degrees of freedom. The generalized coordinates that describe the state of the robot and its motion are denoted by q_i. The dynamic model of the robot is

$$H(\mathbf{q})\ddot{\mathbf{q}} + C(\mathbf{q},\dot{\mathbf{q}}) + g(\mathbf{q}) = \tau\,, \tag{17}$$

where **H**, **C** and **g** denote the inertia matrix, the vector of Coriolis and centrifugal forces and the vector of gravity forces, respectively. **τ** is the vector of the joint torques and **q** is the vector of the joint positions. The dynamic equation does not consider the friction in the gears. For this purpose, an additional controller was implemented in the control strategy.

3.2.1 Description of model using SD/FAST

SD/FAST is a physically-based simulation tool for simulating the mechanical systems. Based on the short description of an articulated mechanical system of rigid bodies it derives the full nonlinear equations of motion for the given system. These equations can then be directly used in a C programming language and further compiled or linked with an arbitrary simulation or animation environment. The symbolic derivation of the equations provides one of the fastest possible simulations of the mechanical system.

		On the ground	In the air
segment	connected	joint type	joint type
foot	ground	rot	2 trans + 1 rot
shank	foot	rot	rot
thigh	shank	rot	rot
trunk	thigh	rot	rot
Number of DOFs		4 (q_3-q_6)	6 (q_1-q_6)

Table 2. Description of the jumping robot

When the system was completely described, SD/FAST generated the equations of motion for both models. To perform simulations and to control the robotic system, these equations were then used in the simulation environment.

3.3 Simulation and control

The equations of motion which were generated by SD/FAST have to be used together with a programming tool that provides the integration of the equations of motion. For this purpose we used Matlab/Simulink. The C code describing the equations of motion is used in S-function, that can be used directly as a Simulink block. We designed two S-functions, one for the inverse dynamics and one for the direct dynamics.

3.3.1 Inverse dynamics

Depending on the current state of the robot ($\mathbf{q},\dot{\mathbf{q}}$) the inverse dynamics block in Simulink defines the matrices **H**, **C** and **g** that form the dynamic equations of motion (17). The inverse dynamics block also defines the position of the COM and its Jacobian matrix, which is used

in the controller. The output of the inverse dynamics block depends on whether the robot is in the contact with the ground or in the air.
To get the requested output of the block, the following SD/FAST functions were used: *sdpos* for the position, *sdrel2cart* to calculate the Jacobian matrix and *sdmassmat*, *sdequivht*, *sdfrcmat* to calculate the **H**, **C** and **g** matrices..

3.3.2 Direct dynamics

The direct dynamic model performs the integration of the equations of motion (17) and returns the states of the robot ($\mathbf{q}, \dot{\mathbf{q}}$) depending on the input torque $\boldsymbol{\tau}$. In our case where Matlab/Simulink performs the integration, we only have to define the derivatives of the states ($\mathbf{q}, \dot{\mathbf{q}}$). To calculate the derivatives of the states and to apply the input torque, the following functions were used: *sdstate* to get states, *sdderiv* to get the derivatives of the states and *sdhinget* to set the torque.

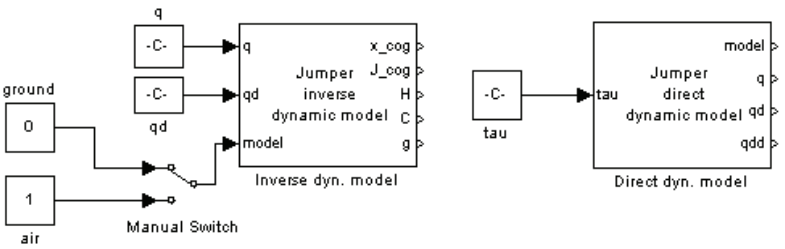

Fig. 6. Inverse and direct dynamic model blocks in simulation environment Simulink

Special attention should be paid to switching between the dynamic models. Usually all movements start with the foot touching the ground. In case of vertical jumping the switch occurs when the ground reaction forces exerted by the robot in the vertical direction change direction from downwards to upwards. In the moment of the switch all joint states have to maintains their values. Hence continuity and dynamic consistency is achieved.
On the other hand when the robot lands, a force impact occurs and the joint velocities change their values. The joint velocities after the impact have to be calculated with regard to the robot configuration and the joint velocities before the impact using following equation (Zheng & Hemami, 1985):

$$\Delta\dot{\mathbf{q}} = \boldsymbol{H}_{\text{air}}^{-1}\boldsymbol{S}^{\mathrm{T}}(\boldsymbol{S}\boldsymbol{H}_{\text{air}}^{-1}\boldsymbol{S}^{\mathrm{T}})^{-1}\Delta\mathbf{v}, \tag{18}$$

where $\mathbf{H}_{\text{air}}$ represents the **H** matrix of the system in the air, $\Delta\mathbf{v}$ represents the velocity change in the moment of the impact and $\Delta\dot{\mathbf{q}}$ represents the resulting changes of the joint velocities at the impact. Matrix **S** defines the constraints of the impact and is equal to

$$\boldsymbol{S} = \begin{bmatrix} 1 & 0 & 0 & 0 & 0 & 0 \\ 0 & 1 & 0 & 0 & 0 & 0 \end{bmatrix}. \tag{19}$$

To get the ground reaction force and the position of the toe, the following functions are used: *sdreac* to calculate the reaction force and *sdpos* to calculate the position.

3.3.3 Control of the system

To control the robot to perform the vertical jump, two separate controllers were used, one for the push-off phase of the jump and the other for the flight phase of the jump. Furthermore, not all degrees of freedom of the robot can be actuated. Both degrees of freedom that describe the position of the toe (q_1 and q_2) and the degree of freedom in the passive toe joint (q_3) are considered as free degrees of freedom that cannot be actuated by the robot. While the robot is in contact with the ground, position of the toe (q_1 and q_2) is fixed. In the free degrees of freedom the control torque should remain zero at all times. The system of dynamic equations that describe the robot can be divided into two parts, for actuated and inactivated joints separately,

$$\begin{bmatrix} \boldsymbol{H}_{11} & \boldsymbol{H}_{12} \\ \boldsymbol{H}_{21} & \boldsymbol{H}_{22} \end{bmatrix} \begin{bmatrix} \ddot{\mathbf{q}}_1 \\ \ddot{\mathbf{q}}_2 \end{bmatrix} + \begin{bmatrix} \boldsymbol{C}_1 \\ \boldsymbol{C}_2 \end{bmatrix} + \begin{bmatrix} \boldsymbol{g}_1 \\ \boldsymbol{g}_2 \end{bmatrix} = \begin{bmatrix} \boldsymbol{\tau}_1 \\ \boldsymbol{\tau}_2 \end{bmatrix}, \tag{20}$$

where $\boldsymbol{\tau}_1$ represents the degrees of freedom that cannot be actuated. This condition leads to

$$\begin{aligned} \boldsymbol{H}_{11}\ddot{\mathbf{q}}_1 + \boldsymbol{H}_{12}\ddot{\mathbf{q}}_2 + \boldsymbol{C}_1 + \boldsymbol{g}_1 &= 0, \\ \boldsymbol{H}_{21}\ddot{\mathbf{q}}_1 + \boldsymbol{H}_{22}\ddot{\mathbf{q}}_2 + \boldsymbol{C}_2 + \boldsymbol{g}_2 &= \boldsymbol{\tau}_2. \end{aligned} \tag{21}$$

Accelerations in the uncontrollable joints $\ddot{\mathbf{q}}_1$ are unknown and can therefore be eliminated. Combining both equations (21) we get

$$\ddot{\mathbf{q}}_1 = -\boldsymbol{H}_{11}^{-1}(\boldsymbol{H}_{12}\ddot{\mathbf{q}}_2 + \boldsymbol{C}_1 + \boldsymbol{g}_1) \tag{22}$$

and

$$-\boldsymbol{H}_{21}\boldsymbol{H}_{11}^{-1}(\boldsymbol{H}_{12}\ddot{\mathbf{q}}_2 + \boldsymbol{C}_1 + \boldsymbol{g}_1) + \boldsymbol{H}_{22}\ddot{\mathbf{q}}_2 + \boldsymbol{C}_2 + \boldsymbol{g}_2 = \boldsymbol{\tau}_2. \tag{23}$$

Finally we get

$$\begin{aligned} &\underbrace{(-\boldsymbol{H}_{21}\boldsymbol{H}_{11}^{-1}\boldsymbol{H}_{12} + \boldsymbol{H}_{22})}_{\boldsymbol{H}_{new}}\ddot{\mathbf{q}}_2 + \\ &\underbrace{(-\boldsymbol{H}_{21}\boldsymbol{H}_{11}^{-1}\boldsymbol{C}_1 + \boldsymbol{C}_2)}_{\boldsymbol{C}_{new}} + \\ &\underbrace{(-\boldsymbol{H}_{21}\boldsymbol{H}_{11}^{-1}\boldsymbol{g}_1 + \boldsymbol{g}_2)}_{\boldsymbol{g}_{new}} = \boldsymbol{\tau}_2. \end{aligned} \tag{24}$$

We have acquired a new dynamic model with three degrees of freedom. The other degrees of freedom cannot be controlled directly; however they can be controlled indirectly using other conditions such as COM and ZMP.

3.3.4 Vertical jump controller

To assure the verticality of the jump, the robot's COM has to move in the upward direction above the support polygon during the push-off phase of the jump. The second condition, which refers to the balance of the robot during the push-off phase, is the position of the zero moment point (ZMP). Both conditions are described in details in (Babič et al. 2006).

The vertical jump consists of a phase when the robot is in contact with the ground and a phase when the robot is in the air without any contact with the environment. To sufficiently

control the vertical jump we used ground model of the robot in the former case and air model of the robot in the latter case. Switching between the models was performed by the controller on the basis of the foot switch.

In the push-off phase of the jump we controlled the position of the COM and ZMP in such a way that the robot performed a vertical jump. The task of the controller in the flight phase of the jump was to stop the motion in all joints and to prevent the mechanical damage by over extension of the joints. At this point we did not consider any strategies for the landing phase of the jump.

To control all joints we used the controller described by

$$\boldsymbol{H}_{new}\ddot{\mathbf{q}}_{2c} + \boldsymbol{C}_{new} + \boldsymbol{g}_{new} = \boldsymbol{\tau}_{2c}, \tag{25}$$

where $\boldsymbol{\tau}_{2c}$ is the control torque and $\ddot{\mathbf{q}}_{2c}$ is the control acceleration of all active degrees of freedom. $\ddot{\mathbf{q}}_{2c}$ is defined as

$$\ddot{\mathbf{q}}_{2c} = \ddot{\mathbf{q}}_{2d} + K_p\mathbf{e} + K_d\dot{\mathbf{e}}, \quad \mathbf{e} = \mathbf{q}_{2d} - \mathbf{q}_2. \tag{26}$$

Here, $\mathbf{q}_{2d}$ and $\mathbf{q}_2$ are the desired and the actual joint positions of the joints, respectively. The desired joint trajectory during the jump is defined with regard to the COM and ZMP as described in (Babič et al. 2006).

Fig. 7 schematically shows the complete system consisting of the controller and the direct dynamic model of the robot. The controller includes both ground and air controllers of the vertical jump. These two controllers are merged together as shown in Fig. 8.

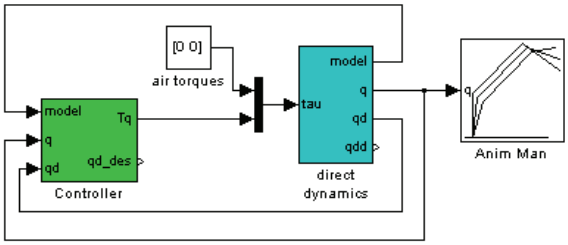

Fig. 7. Block diagram of robotic system consisting of controller and direct dynamic model of robot

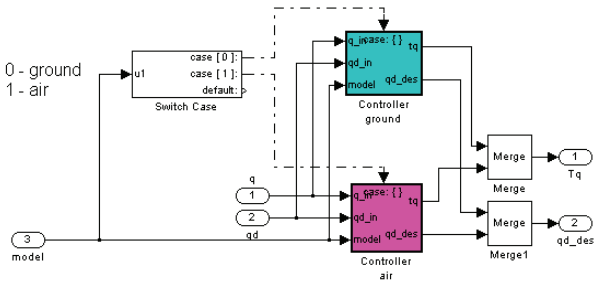

Fig. 8. Block diagram of vertical jump controller made of two separate controllers for push-off and flight phases of vertical jump

3.4 Vertical jump experiments

Based on the numerical results, we performed vertical jumping experiments with the hardware prototype and the controller described above. Joint torques obtained in the simulation study were used as the desired joint torques for the experiments. In the first case we performed squat vertical jumps for a conventional robot that does not have a biarticular link. In the second case we performed squat vertical jumps for a biarticular legged robot. In this latter case the robot was equipped with biarticular link that represents the gastrocnemius muscle in a human leg.

The robot performed jumps on a force platform that was used to measure ground reaction forces generated by the robot during the push-off and landing phases of the vertical jump. By double integration of the measured forces that are proportional to the acceleration of the robot's center of mass during the jump, the trajectory of the robot's center of mass is determined during the vertical jump experiments. In this way we obtained the height of the jump of the robot without the biarticular link (0.11m) and the height of the jump of the biarticular legged robot (0.13m). The biarticular legged robot jumped approximately 18% higher than the conventional robot.

A typical sequence of the vertical jump performed by the biarticular legged robot is shown in Fig. 9. Images in the first row show the robot between the beginning of the push-off phase of the jump and the moment when the robot reached the maximal height of the jump. In the second row of Fig. 9 the second part of the flight phase and the landing phase is shown.

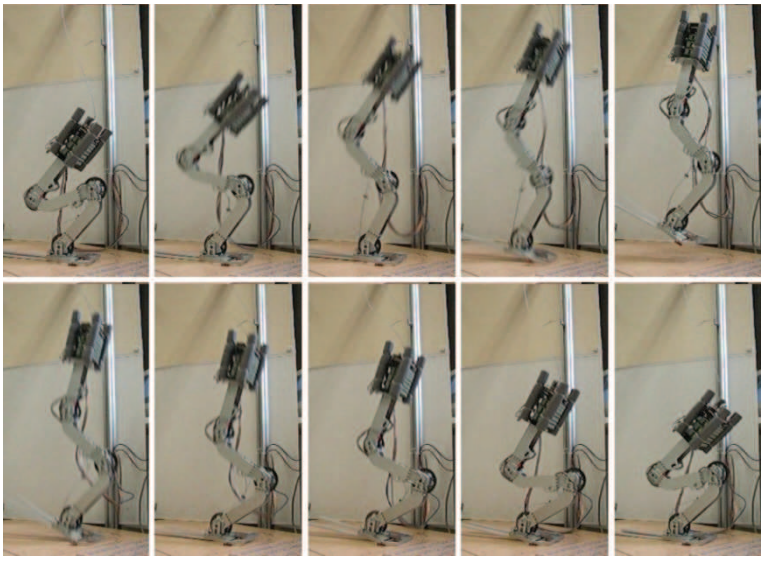

Fig. 9. A sequence of the biarticular legged robot performing a vertical jump experiment

4. Acknowledgement

This investigation was supported by the Slovenian Ministry of Education, Science and Sport. Thanks to Borut Lenart, Jožef Stefan Institute for designing the robot prototype and to Damir Omrčen, Jožef Stefan Institute for designing the vertical jump controller and for the help with the experiments.

5. References

Alexander, R.McN. (1988). *Elastic mechanisms in animal movement,* Cambridge University Press, Cambridge

Asada, H. & Slotine, J.J.E. (1986). *Robot analysis and control*, John Wiley and sons, New York

Asmussen, E. & Bonde-Petersen, F. (1974). Storage of elastic energy in skeletal muscles in man. *Acta Physiologica Scandinavica*, 91, 385-392

Audu, M.L. & Davy, D.T. (1985). The influence of muscle model complexity in musculoskeletal motion modeling. *Journal of Biomechanical Engineering*, 107, 147-157

Babič, J. & Lenarčič, J. (2004). In vivo determination of triceps surae muscle-tendon complex viscoelastic properties. *European Journal of Applied Physiology*, 92, 477-484

Babič, J., Omrčen, D. & Lenarčič, J. (2006). Balance and control of human inspired jumping robot, *Advances in Robot Kinematics*, J. Lenarčič, B. Roth (Eds.), pp. 147-156, Springer

Babič, J.; Karčnik, T. & Bajd, T. (2001). Stability analysis of four-point walking, *Gait & Posture*, 14, 56-60

Bobbert, M.F.; Gerritsen, K.G.M.; Litjens, M.C.A. & Soest, A.J. van (1996). Why is countermovement jump height greater than squat jump height? *Medicine & Science in Sports & Exercise*, 28, 1402-1412

Bobbert, M.F.; Hoed, E.; Schenau, G.J. van.; Sargeant, A.J. & Schreurs, A.W. (1986). A model to demonstrate the power transportating role of bi-articular muscles, *Journal of Physiology,* 387 24

Bogert, A.J. van den; Hartman, W.; Schamhardt, H.C. & Sauren, A.A. (1989). In vivo relationship between force, EMG and length change in the deep digital flexor muscle in the horse, In *Biomechanics XI-A,* G. de Groot; A.P. Hollander; P.A. Huijing; G.J. van Ingen Schenau (Eds.), pp. 68-74, Free University Press, Amsterdam

Brand, R.A.; Crowninshield, R.D.; Wittstock, C.E.; Pederson, D.R.; Clark, C.R. & Krieken, F.M. van (1982). A model of lower extremity muscular anatomy. *Journal of Biomechanics*, 104, 304-310

Cavagna, G.A. (1970). Elastic bounce of the body, *Journal of Applied Physiology*, 29, 279-282

Davy, D.T. & Audu, M.L. (1987). A dynamic optimization technique for predicting muscle forces in the swing phase of gait. *Journal of Biomechanics*, 20, 187-201

Delp, S.L. (1990). Surgery simulation: A computer graphics system to analyze and design musculoskeletal reconstructions of the lower limb, Doctoral Dissertation, Stanford University, Palo Alto

De Man, H., Lefeber, F., Daerden, F. & Faignet, E. (1996). Simulation of a new control algorithm for a one-legged hopping robot (using the multibody code mechanics motion), In *Proceedings International Workshop on Advanced Robotics and Intelligent Machines*, pp.1-13

Hyon, S., Emura, T. & Mita, T. (2003). Dynamics-based control of a one-legged hopping robot, *Journal of Systems and Control Engineering*, 217, 83–98

Hobara, H. (2008). Spring-like leg behavior and stiffness regulation in human movements, Coctoral Dissertation, Waseda University, Japan

Iida, F., Minekawa, Y., Rummel, J., Seyfarth, A. (2009). Toward a human-like biped robot with complient legs. *Robotics and Autonomous Systems*, 57, 139-144

Ker, R.F.; Bennett, M.B.; Bibby, S.R.; Kester, R.C. & Alexander, R.McN. (1987). The spring in the arch of the human foot. *Nature*, 325, 147-149

Legreneur, P.; Morlon, B. & Hoecke, J. van (1997). Joined effects of pennation angle and tendon compliance on fibre length in isometric contractions: A simulation study. *Archives of Physiology and Biochemistry*, 105, 450-455

Leva, P. de (1996). Adjustments to Zatsiorsky-Seluyanov's segment inertia parameters. *Journal of Biomechanics*, 29, 1223-1230

Raibert, M. (1986). *Legged Robots That Balance*, MIT Press.

Schenau, G.J. van. (1989). From rotation to translation: constraints of multi-joint movements and the unique action of bi-articular muscles, *Human Movement Science*, 8, 301-337

Shorten, M.R. (1985). Mechanical energy changes and elastic energy storage during treadmill running, In: *Biomechanics IXB*, D.A. Winter; R.W. Norman; R. Wells; K.C. Hayes; A. Patla (Eds.), pp. 65-70, Human Kinetics Publ, Champaign

Zatsiorsky, V. & Seluyanov, V. (1983). The mass and inertia characteristics of the main segments of the human body, In *Biomechanics VIII-B,* H. Matsui; K. Kobayashi (Eds.), pp. 1152-1159, Human Kinetics, Illinois

Zheng, Y.F. & Hemami, H. (1985). Mathematical modeling of a robot collision with its environment, *Journal of Robotic Systems,* 2, 289-307

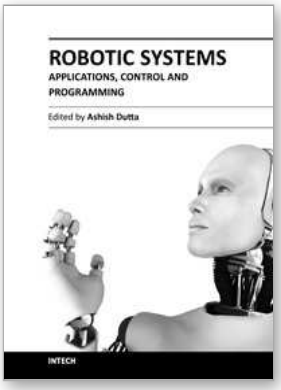

Robotic Systems - Applications, Control and Programming
Edited by Dr. Ashish Dutta

ISBN 978-953-307-941-7
Hard cover, 628 pages
Publisher InTech
Published online 03, February, 2012
Published in print edition February, 2012

This book brings together some of the latest research in robot applications, control, modeling, sensors and algorithms. Consisting of three main sections, the first section of the book has a focus on robotic surgery, rehabilitation, self-assembly, while the second section offers an insight into the area of control with discussions on exoskeleton control and robot learning among others. The third section is on vision and ultrasonic sensors which is followed by a series of chapters which include a focus on the programming of intelligent service robots and systems adaptations.

InTech Europe
University Campus STeP Ri
Slavka Krautzeka 83/A
51000 Rijeka, Croatia
Phone: +385 (51) 770 447
Fax: +385 (51) 686 166
www.intechopen.com

InTech China
Unit 405, Office Block, Hotel Equatorial Shanghai
No.65, Yan An Road (West), Shanghai, 200040, China
中国上海市延安西路65号上海国际贵都大饭店办公楼405单元
Phone: +86-21-62489820
Fax: +86-21-62489821